
Adversarial Dependence Minimization

Pierre-François De Plaen¹ Tinne Tuytelaars¹ Marc Proesmans¹ Luc Van Gool^{1 2 3}

Abstract

Many machine learning techniques rely on minimizing the covariance between output feature dimensions to extract minimally redundant representations from data. However, these methods do not eliminate all dependencies/redundancies, as linearly uncorrelated variables can still exhibit nonlinear relationships. This work provides a differentiable and scalable algorithm for dependence minimization that goes beyond linear pairwise decorrelation. Our method employs an adversarial game where small networks identify dependencies among feature dimensions, while the encoder exploits this information to reduce dependencies. We provide empirical evidence of the algorithm’s convergence and demonstrate its utility in three applications: extending PCA to nonlinear decorrelation, improving the generalization of image classification methods, and preventing dimensional collapse in self-supervised representation learning.

1. Introduction

In representation learning (Rumelhart et al., 1986b; Hinton et al., 2006; Bengio et al., 2013), algorithms learn to extract lower-dimensional encodings from input data, aiming for compact yet informative representations. A key strategy is to learn representations with minimally redundant dimensions, where each feature encodes a distinct concept. Such minimally redundant dimensions may offer several advantages: efficient data compression, improved generalization to unseen data, enhanced interpretability of the learned representations, ...

The strategy of minimizing feature redundancy has been applied in various methods, from classical techniques like the Principal Component Analysis (Pearson, 1901; Hotelling, 1933) to more recent self-supervised learning

¹ESAT-PSI, KU Leuven, Belgium ²CVL, ETH Zürich, Switzerland ³INSAIT, Sofia University, Bulgaria. Correspondence to: Pierre-François De Plaen <pdeplaen@esat.kuleuven.be>.

(SSL) approaches (Huang et al., 2018; Zbontar et al., 2021; Bardes et al., 2021). Both PCA and these SSL methods aim to extract representations with uncorrelated dimensions. However, it is important to note that while these methods minimize pairwise linear correlations (ρ) between embedding dimensions, non-linear dependencies may still be present. We illustrate this with Example 1 (Figure 1b).

Example 1. Let a random variable x_1 be drawn from a uniform distribution over the interval $[-a, a]$ and $x_2 = x_1^2$. Since x_2 is a deterministic function of x_1 , it is clear that the variables co-vary. However, we find that: $\text{Cov}(x_1, x_2) = 0$ and $\rho(x_1, x_2) = 0$. The random variables are thus dependent despite zero correlation.

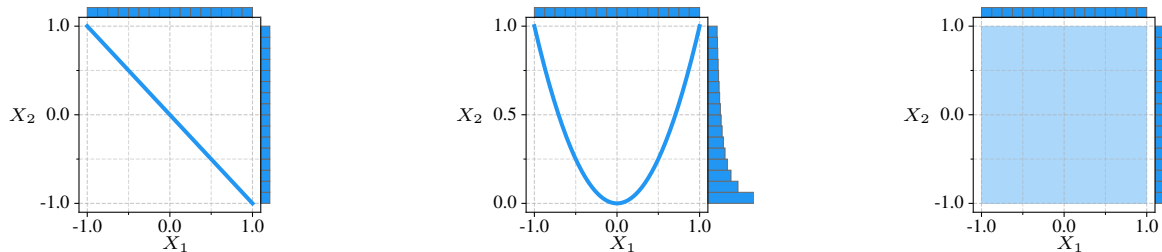
This example highlights a limitation of algorithms that rely on Pearson correlation: they may not eliminate all forms of dependencies/redundancies, as linearly uncorrelated variables can still exhibit nonlinear relationships (Hyvärinen & Oja, 2000). Still, developing a stable method for mutual and nonlinear dependence reduction remains an unresolved problem. The challenge lies in designing a training objective that is simultaneously differentiable, scalable, and distribution-agnostic.

This paper presents a training algorithm to reduce the dependence among learned embedding dimensions using neural networks. The algorithm involves an adversarial game between two types of players: (1) a series of small neural networks are trained to predict one dimension of a representation given the other dimensions, and (2) an encoder is trained to counter reconstruction by updating the representations.

Our adversarial objective can be viewed as a soft independence constraint in a task-specific optimization problem, allowing its incorporation into various learning algorithms. In this work, we explore three potential applications:

1. extending the PCA algorithm to non-linear decorrelation (unsupervised learning)
2. learning features that generalize beyond label supervision in supervised learning
3. preventing dimensional collapse in SSL by learning minimally redundant representations

This paper’s main contribution is the introduction of an algorithm for nonlinear mutual dependence minimization



(a) Lin. $x_2 = -x_1$: $\rho = -1$ and $\mathcal{R} = 1$. (b) Nonlin. $x_2 = x_1^2$: $\rho = 0$ and $\mathcal{R} = \sqrt{1/2}$. (c) Indep. $x_2 \in \mathcal{U}(-1, 1)$: $\rho = \mathcal{R} = 0$.

Figure 1: Illustration of the joint and marginal distributions for different types of dependencies between random variables $x_1 \in \mathcal{U}(-1, 1)$ and X_2 . The variables are linearly uncorrelated ($\rho = 0$) in both (b) and (c) but are independent only in (c).

and showing that, when combined with a standardization of the representations, it systematically converges to an equilibrium where the dependence among the embedding dimensions is minimal. In addition, we (1) illustrate the extension of the PCA algorithm with an example, (2) provide an alternative formulation that allows for a small degree of redundancy, and run experiments that suggest that this formulation helps a classification model learn concepts beyond label supervision, and finally (3) show how our SSL method generalizes current SSL decorrelation techniques, and analyze its benefits and shortcomings.

2. Related Work

The Principal Component Analysis (PCA) was the first dimensionality reduction technique that focused on extracting uncorrelated features. This transformation is achieved while preserving the maximal variance in the original dataset.

Autoencoders (AEs). The PCA reduction is closely related to autoencoders (Kramer, 1991; Rumelhart et al., 1986a). An AE consists of two neural networks: an encoder that compresses the input into a lower-dimensional code, and a decoder that reconstructs the input from this representation. Both networks are trained jointly with a reconstruction error. Interestingly, the optimal solution of a linear AE corresponds to performing PCA. However, unlike PCA, an autoencoder can learn nonlinear dimensionality reductions, but its latent space is not guaranteed to have uncorrelated dimensions. The variational autoencoder (VAE, (Kingma, 2013)) is an extension of AEs in which the encoder maps the input data into a probabilistic representation and the decoder reconstructs data by sampling from this distribution. This extension of AEs enabled the generation of new samples similar to the training data. Multiple works (Higgins et al., 2017; Burgess et al., 2018; Kim & Mnih, 2018; Chen et al., 2018) proposed variations of the VAE objective to encourage disentangled representations. Intuitively, disentanglement implies learning repre-

sentations where changes in one dimension correspond to changes in a single latent variable, but disentangled concepts may be dependent. From this perspective, the problem is ill-defined (Locatello et al., 2019) and is not the focus of this study.

Independent Component Analysis (ICA). ICA (Jutten & Herault, 1991) is a method to separate mixed signals into independent ones. Unlike PCA, ICA does not reduce dimensionality but instead focuses on identifying statistically independent components. When combined with an AE, our dependence minimization algorithm solves a combination of PCA and ICA. However, the successive application of PCA and ICA (Back & Weigend, 1997; Yao et al., 2012) is not equivalent to our approach since the PCA decomposition may extract redundant features on which ICA is then ill-posed.

Self-supervised learning (SSL). SSL is an active research area in the field of representation learning. Popularized by SimCLR (Chen et al., 2020), a leading paradigm in SSL is to train a network to be invariant under carefully designed data augmentations (such as illumination changes, cropping, ...). While effective, this idea comes with the risk of collapsed representations (Hua et al., 2021): dimensional collapse and collapse to a single value. The former happens when embedding vectors span a lower-dimensional subspace instead of the entire available space (Jing et al., 2022), while the latter is generally due to a lack of counterweight to the invariance term. Many SSL approaches relied on linear decorrelation of output dimensions (Huang et al., 2018; Zbontar et al., 2021; Ermolov et al., 2021; Bardes et al., 2021) as a means to avoid collapse. However, as illustrated in Example 1, linearly uncorrelated dimensions can still co-vary. Our algorithm extends the idea to nonlinear mutual dependence minimization, and finds a broader scope of applications.

Input-output mutual information maximization. Another line of work on dimensionality reduction is based on the infomax principle (Linsker, 1988; Bell & Sejnowski,

1995), which suggests maximizing the mutual information (MI) between the input data and the output of a neural network to learn informative representations. Mutual Information Neural Estimation (MINE, (Belghazi et al., 2018)) provided a first estimate of the MI between high-dimensional continuous random variables using neural networks. Based on MINE, DeepInfoMax (Hjelm et al., 2019) learns representations by: maximizing the input-output MI, maximizing the MI between global and local representations, and matching the output to a uniform prior with adversarial learning. Similarly to our work’s objective, MI is an information-theoretic measure of the information shared by two random variables. However, our algorithm does not explicitly maximize input-output MI but instead minimizes the MI between output dimensions.

Adversarial learning. We now discuss the core training paradigm behind our algorithm. Generative Adversarial Networks (GANs, (Goodfellow et al., 2014)) are the first approach to training neural networks adversarially: a generator is trained to create realistic synthetic data, while a discriminator is trained to predict whether a sample came from the training dataset or the generator. InfoGANs (Chen et al., 2016) extends GANs by adding a criterion that maximizes a lower bound of the MI between the representations and the generated data. This helps learn disentangled representations. Our approach differs from InfoGANs as it does not maximize a proxy for MI and it is not bound to generative networks. Most similar to our work, (Brakel & Bengio, 2017) used adversarial networks to decrease dependence by training an encoder to produce samples from a joint distribution that are indistinguishable from samples of the product of its marginals. However, this training objective is unstable and requires careful tuning, whereas ours systematically converges to the desired equilibrium.

3. Background and Motivation

We begin by defining the notion of statistical independence, before highlighting two shortcomings of current methods.

Let x_1, \dots, x_d be a finite set of random variables. These variables are mutually independent if and only if:

$$F_{x_1, \dots, x_d}(x_1, \dots, x_d) = \prod_{i=1}^d F_{x_i}(x_i) \quad \forall x_1, \dots, x_d \in \mathbb{R} \quad (1)$$

where F_{x_1, \dots, x_d} is the joint cumulative distribution function and F_{x_i} are the marginal cumulative distribution functions. Similarly, two continuous random variables x_1 and x_2 are pairwise independent if and only if their joint cumulative distribution function is equal to the product of their cumulative distribution functions. It is worth highlighting that random variables can all be pairwise independent without being mutually independent (Driscoll, 1978). We refer to

Appendix C.2 for an example.

The statistical dependence between two random variables can be measured by correlation. The term generally refers to Pearson’s correlation coefficient, which captures the degree of linear dependence between a pair of random variables. However, it fails to capture non-linear dependencies; thus, a zero correlation does not imply independence.

Therefore, one must consider mutual and non-linear dependencies when designing an algorithm to minimize redundancy among feature dimensions.

Finally, a metric is required to estimate correlations beyond linearity. Distance correlation (Székely et al., 2007) is a non-negative coefficient that characterizes both linear and nonlinear correlations between random vectors by measuring the distance between their joint characteristic function and the product of the marginal characteristic functions. For more details, see Appendix C.1. Of particular interest, the distance correlation is zero $\mathcal{R}(x_1, x_2) = 0$ if and only if x_1 and x_2 are independent. Returning to Example 1, we find a nonzero distance correlation between the random variables: $\mathcal{R}(x_1, x_2) = \sqrt{1/2}$.

4. Adversarial Dependence Minimization

We present the *Adversarial Dependence Minimization* (ADMin) algorithm to reduce the nonlinear mutual dependence among learned embedding dimensions.

Consider the representations $z^{(i)} = f_{\theta}(x^{(i)})$ from input samples $x^{(i)}$ of a dataset $\mathbf{X} = \{x^{(i)}\}_{i=1}^N$ with i.i.d. samples. Our algorithm involves two types of networks: an encoder $f_{\theta} : \mathcal{X} \rightarrow \mathbb{R}^d$ that learns lower-dimensional representations of the training data and a small *dependency predictor* for every embedding dimension $h_{\phi_i} : \mathbb{R}^{d-1} \rightarrow \mathbb{R}$. The *dependency predictors* are trained to learn how dimensions relate by imputing a missing value z_i based on the other values z_{-i} :

$$\hat{z}_i = h_{\phi_i}(z_{-i}) = h_{\phi_i}(z_1, \dots, z_{i-1}, z_{i+1}, \dots, z_d) \quad (2)$$

Importantly, each network takes all $d - 1$ remaining dimensions as input to effectively capture mutual dependencies. We implement *dependency predictors* with Multi-Layer Perceptrons (MLP) since they are universal approximators (Hornik et al., 1989; Cybenko, 1989; Leshno et al., 1993) and can, in theory, approximate arbitrarily well the relation among the variables if given enough capacity.

Intuitively, we now aim to design an algorithm that would exploit the knowledge extracted by the *dependency predictors* to guide the encoder to reduce the dependence among the embedding dimensions. Taking inspiration from Generative Adversarial Networks (Goodfellow et al., 2014), we train both networks simultaneously and model the objec-

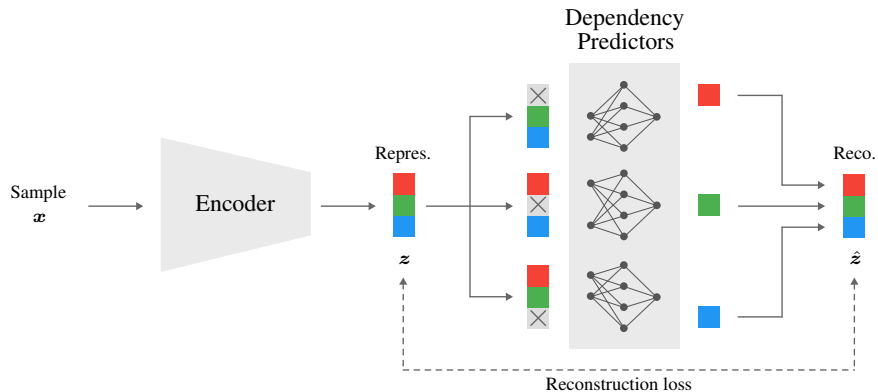


Figure 2: Illustration of the *adversarial dependence minimization* architecture. The *dependency predictors* minimize the reconstruction error by learning how dimensions relate, while the encoder maximizes the error by reducing dependencies.

tive as a two-player game where the encoder and *dependency predictors* are respectively trained to maximize and minimize the expected reconstruction error:

$$\min_{\phi} \max_{\theta} \mathbb{E}_{z \sim P(\mathcal{X}; \theta)} \|z - \hat{z}\|_2^2 \quad (3)$$

where $P(\mathcal{X}; \theta)$ is the distribution of representations learned by the encoder, parameterized by θ . In this adversarial game (depicted in Figure 2), the *dependency predictors* learn how dimensions relate by minimizing the reconstruction error (\min_{ϕ}), while the encoder maximizes the error (\max_{θ}) by exploiting this information to reduce dependencies.

Linear example. Take for instance linear dependency networks: each network will learn affine relations among the representation’s dimensions to reconstruct the remaining one accurately. However, a linear network cannot succeed when the output dimensions are affinely independent. Therefore, training an encoder to counter the reconstruction can be interpreted as a proxy objective for the decorrelation of the dimensions.

Efficient implementation. Since running many small *dependency predictors* sequentially is inefficient on GPUs, we concatenate the inputs from the d networks and implement the dependency networks as one large convolutional network with one-dimensional grouped convolutions (Krizhevsky et al., 2012) with d groups. This equivalent implementation allows all models to be run at once.

4.1. Standardized Formulation

This section introduces a bounded formulation of the problem that empirically converges to minimally dependent dimensions.

The encoder is trained to maximize the reconstruction error. It may therefore indefinitely enlarge the norm of the representations to increase the error. We overcome this trivial

solution by standardizing the distribution dimension-wise before reconstruction: $z_i \leftarrow (z_i - \mathbb{E}[z_i]) / \sqrt{\mathbb{V}[z_i]}$ where $\mathbb{E}[z_i]$ and $\mathbb{V}[z_i]$ are respectively the mean and variance of dimension i . These quantities are estimated from the current mini-batch, similarly to batch-normalization layers (Ioffe & Szegedy, 2015).

Proposition 4.1. *The adversarial game of Equation 3 converges, under standardized representations, to a solution where the dependence among the dimensions is minimal and where the dependency predictors predict the mean (zero) vector. The average reconstruction error is then equal to the (unit) variance.*

Here follows an intuitive justification of the proposition, which we empirically verify in Section 6.1: if the *dependency predictors* are trained with an MSE reconstruction loss and predict the mean vector, then the expected value of the loss is, by definition, equal to the variance (Baldi & Hornik, 1989). This variance is consistently one for representations standardized to have a zero mean and unit variance. Assuming that the dependency networks can approximate the (fixed) mean, this forms an upper bound on the expected error since it can be achieved regardless of the distribution of representations. The mean is also the prediction with the lowest-cost expected error when embedding dimensions are statistically independent since the input of the *dependency predictors* is then irrelevant to the quantity to estimate. Furthermore, a dependence among the feature dimensions learned by the encoder could lead to a lower cost loss as the dependency networks may exploit the dependence to improve the reconstruction.

Let us further rewrite the adversarial objective from the encoder as the following equivalent minimization problem: $\arg \max_{\theta} \mathbb{E}_{z \sim P(\mathcal{X}; \theta)} \|z - \hat{z}\|_2^2 = \arg \min_{\theta} 1 - \mathbb{E}_{z \sim P(\mathcal{X}; \theta)} \|z - \hat{z}\|_2^2$. This loss is equal to zero when the *dependency predictors* can do no better than predicting the mean since the average expected error is then equal to one.

4.2. Margin Loss Formulation

What if certain applications required representations with a small degree of redundancy? Take, for instance, the following classification problem:

Example 2. Consider a dataset of colored shapes with three training classes: "red squares", "green triangles", and "blue triangles". A classifier could achieve a minimum loss value of zero and perfect accuracy by solely relying on the color. However, when presented with unseen "red triangles" during inference, the model would then confidently misclassify these as "red squares", despite the different shape.

Fixing the limitation in Example 2 requires the classifier to extract features for both *shape* and *color*, which could be encouraged by minimizing redundancy in the output representation. Unfortunately, the two latent variables are not statistically independent in the training set. Indeed, assuming a balanced number of samples in every class, we find $P(\text{"green"} \cap \text{"triangle"}) = \frac{1}{3}$ and $P(\text{"green"})P(\text{"triangle"}) = \frac{1}{3} \cdot \frac{2}{3} = \frac{2}{9}$, so $P(\text{"green"} \cap \text{"triangle"}) \neq P(\text{"green"})P(\text{"triangle"})$.

Hence, we introduce an alternative formulation that only minimizes dependence up to a certain threshold. We formulate the encoder's objective as the maximization of a pairwise margin (Cortes, 1995; Tsochantaridis et al., 2005) with hyper-parameter α : $\min_{\theta} \max(0, \alpha - \|z - \hat{z}\|_2^2)$. With this formulation, the encoder does not push the reconstruction error beyond α , while *dependency predictors* are still trained to minimize the reconstruction error with no margin: $\|z - \hat{z}\|_2^2$.

5. Applications

Having developed an algorithm for interdependence minimization, we explore its applicability in diverse tasks: consider a task-specific minimization problem with objective function $\mathcal{L}_{\text{task}}$ that we would like to restrict to solutions for which the output dimensions are independent:

$$\begin{aligned} \min_{\theta} \quad & \mathcal{L}_{\text{task}}(\mathbf{X}, \cdot; \theta) \\ \text{subject to} \quad & z_1 \perp\!\!\!\perp z_2 \perp\!\!\!\perp \dots \perp\!\!\!\perp z_d \end{aligned} \quad (4)$$

where $\perp\!\!\!\perp$ denotes that each random variable is mutually independent of all others.

We observe that the encoder's objective from Section 4 can be seen as a Lagrangian relaxation of the independence constraint. Indeed, both the standardized and margin formulations can be rewritten as constraints of the form $g(x) = 0$, where the constraint is fulfilled when dimensions are minimally dependent¹. Therefore, the problem

¹Assuming that dependency predictors have enough capacity

from Equation 4 can be relaxed to:

$$\min_{\theta} \mathcal{L}_{\text{task}}(\mathbf{X}, \cdot; \theta) + \lambda \mathcal{L}_{\text{adv}}(\mathbf{Z}, \hat{\mathbf{Z}}; \theta, \phi) \quad (5)$$

where $\lambda \in \mathbb{R}$ is a Lagrange multiplier and where the adversarial objective from the encoder is denoted by $\mathcal{L}_{\text{adv}}(z, \hat{z}) = 1 - \|z - \hat{z}\|_2^2$ for the standardized formulation or by $\mathcal{L}_{\text{adv}}(z, \hat{z}) = \max(0, \alpha - \|z - \hat{z}\|_2^2)$ for the margin loss formulation.

In this approximated objective, the soft constraint pushes towards minimally dependent embedding dimensions, and thus minimally redundant solutions. In the following, we investigate three applications for this objective: an extension of PCA to nonlinear decorrelation (Section 5.1), the minimization of redundancy in a supervised classification setting (Section 5.2) and the use of the algorithm to prevent dimensional collapse in SSL (Section 5.3).

5.1. Principal and Independent Component Analysis

PCA is a linear dimensionality reduction technique that transforms a set of variables $\mathbf{X} = \{\mathbf{x}^{(i)}\}_{i=1}^N$, $\mathbf{x}^{(i)} \in \mathbb{R}^l$ into a set of uncorrelated representations $\mathbf{z}^{(i)} = \mathbf{W}^T \mathbf{x}^{(i)}$, $\mathbf{z}^{(i)} \in \mathbb{R}^d$, where the columns of the matrix $\mathbf{W} \in \mathbb{R}^{l \times d}$ are called principal components. Intuitively, PCA identifies directions $\mathbf{W}_{:,i}$ in the input space along which the variance of the projected data is maximized. Assuming centered data, the PCA reduction solves the following problem:

$$\max_{\mathbf{W}} \frac{1}{N-1} \sum_{i=1}^N \|\mathbf{W}^T \mathbf{x}^{(i)}\|_2^2 \quad \text{s.t.} \quad \mathbf{W}^T \mathbf{W} = \mathbf{I}_d \quad (6)$$

We proceed to discuss two key properties of PCA. Firstly, the orthogonality constraint on the projection matrix \mathbf{W} ensures that the dimensions of the projections are uncorrelated: $\text{Cov}(z_i, z_j) = 0$ for all $i \neq j$. Secondly, PCA can equivalently be defined as finding the projection matrix minimizing the MSE for reconstructions $\hat{\mathbf{x}}^{(i)} = \mathbf{W} \mathbf{z}^{(i)} = \mathbf{W} \mathbf{W}^T \mathbf{x}^{(i)}$. This dual form led to the use of autoencoders to solve PCA (Baldi & Hornik, 1989; Kramer, 1991; Hinton & Salakhutdinov, 2006). It is worth observing that the constraint on the unit norm of the principal components is not needed in the dual formulation, as the reconstruction error inherently accounts for the scale of the projections.

Given these observations, we extend the PCA algorithm to non-linear decorrelation by replacing the covariance constraint with our more general (standardized) dependence minimization objective:

$$\min_{\mathbf{W}} \frac{1}{N} \sum_{i=1}^N \|\mathbf{x}^{(i)} - \mathbf{W} \mathbf{z}^{(i)}\|_2^2 + \lambda \mathcal{L}_{\text{adv}}(\mathbf{z}^{(i)}, \hat{\mathbf{z}}^{(i)}) \quad (7)$$

and that the dependence is minimal when dependency predictors are fooled.

In the following, we illustrate the relevance of this PCA extension with a simple example and refer to it as *Principal and Independent Component Analysis* (PICA).

Example 3. let two independent latent factors v_1 and v_2 be uniformly distributed over the interval $[-\sqrt{3}, \sqrt{3}]$ (so that $\mathbb{V}[v_1] = \mathbb{V}[v_2] = 1$) and observations of a random vector defined by: $\mathbf{x} = [5v_1, 3 \cos(2\pi v_1/\sqrt{3}), v_2]^T$. The observations are linearly uncorrelated by construction: $\text{Cov}[x_i, x_j] = 0$ for all $i \neq j$, and with descending variances: $\mathbb{V}[x_1] = 25$, $\mathbb{V}[x_2] = 9/2$, $\mathbb{V}[x_3] = 1$. Since PCA extracts uncorrelated variables with maximal variance, its solution for $d = 2$ is: $\mathbf{z}_{\text{PCA}} = [x_1, x_2]^T$. Yet, this solution is highly redundant since x_1 and x_2 are both functions of v_1 . In contrast, the global minimum to the PICA objective is the maximum variance solution with independent dimensions: $\mathbf{z}_{\text{PICA}} = [x_1, x_3]^T = [5v_1, v_2]^T$. Unlike the PCA reduction, these learned features capture both true latent factors. We further discuss this example and empirically study its solutions in Appendix A.1.

The PCA extension also holds for non-linear AEs, leading to a NLPKA reduction (Kramer, 1991) with minimal redundancy. We refer interested readers to Appendix A.2.

5.2. Classifiers and Generalization

Example 2 illustrated that a classifier may rely only on a subset of the relevant characteristics to discriminate training classes. We encourage a classifier to minimize redundancy among the embedding dimensions to counter this limitation. This could push the model to encode additional features (e.g., *shape* and *color* in this example) and better generalize. Furthermore, since perfectly independent embedding dimensions may not be optimal for classification, we implement the adversarial objective with the margin loss formulation, which only maximizes the reconstruction error until dependency predictors fail to reconstruct samples with an error lower than a margin α . Formally, the loss function is a weighted combination of the softmax cross-entropy loss and the adversarial objective:

$$\min_{\theta, W, \mathbf{b}} \frac{1}{N} \sum_{i=1}^N \mathcal{L}_{\text{CE}}(\text{softmax}(W\mathbf{z}^{(i)} + \mathbf{b}), y^{(i)}) + \lambda \mathcal{L}_{\text{adv}}(\mathbf{z}^{(i)}, \hat{\mathbf{z}}^{(i)}) \quad (8)$$

where $\mathbf{z}^{(i)} \in \mathbb{R}^d$ is the penultimate representation of the classifier, $y^{(i)}$ is the target class index, $W \in \mathbb{R}^{n_c \times d}$ and $\mathbf{b} \in \mathbb{R}^{n_c}$ are respectively the weights and biases from the classification head with n_c classes.

5.3. Self-Supervised Learning

Following SimCLR (Chen et al., 2020) and the SSL techniques built on it (Zbontar et al., 2021; Caron et al., 2021;

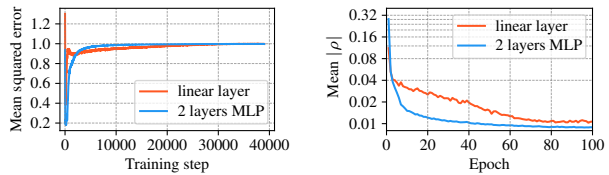


Figure 3: Convergence analysis on TinyImageNet for linear and non-linear *dependency predictors*. **Left:** the reconstruction MSE converges to one. **Right:** logarithmic plot of the average absolute value of the Pearson correlation² on the validation set: correlation decreases over time.

Bardes et al., 2021), we learn representations by training a network to be invariant to data augmentations. Intuitively, it enforces consistency between the input and the output by pushing two augmentations of the same image to lie close in the embedding space, i.e. a small change in the input should not lead to a completely different output. Furthermore, in a similar spirit to decorrelation SSL techniques (Huang et al., 2018; Zbontar et al., 2021), our AD- Min algorithm prevents dimensional collapse (Jing et al., 2022) by pushing representations to be minimally redundant. However, unlike those approaches, ours is not bound to pairwise decorrelation and can thus eliminate all forms of redundancies.

In practice, we sample a mini-batch of n images and duplicate every image. We then apply different data augmentations to the two views of each image and enforce invariance by minimizing the MSE between the representations \mathbf{z} and \mathbf{z}' from corresponding augmented views:

$$\min_{\theta} \frac{1}{N} \sum_{i=1}^N \|\mathbf{z}^{(i)} - (\mathbf{z}')^{(i)}\|_2^2 + \frac{\lambda}{2} \left[\mathcal{L}_{\text{adv}}(\mathbf{z}^{(i)}, \hat{\mathbf{z}}^{(i)}) + \mathcal{L}_{\text{adv}}((\mathbf{z}')^{(i)}, (\hat{\mathbf{z}}')^{(i)}) \right] \quad (9)$$

where invariance is applied to standardized representations following BYOL (Grill et al., 2020).

6. Experiments

Our experimental evaluation aims to: assess the convergence of the algorithm, demonstrate the potential of the supervised and SSL applications on synthetic data, and study the SSL method on real-world data.

6.1. Convergence

This section analyzes the convergence of the adversarial game with standardized representations. Specifically,

²Due to computational constraints, we use Pearson correlation instead of distance correlation for tracking training dynamics.

we trained a ResNet-18 (He et al., 2016) on the Tiny-ImageNet dataset (Le & Yang, 2015) without data augmentations. Both linear and two-layer dependency models were tested. We additionally trained a ResNet-18 encoder and two-layer *dependency predictors* on the ImageNet dataset (Deng et al., 2009) with data augmentations. Detailed experimental setups are provided in Appendix G.1.

Metrics. We reported the average of the absolute value of the Pearson correlation between all pairs of embedding dimensions over time. Additionally, we estimated non-linear dependences with the distance correlation between one dimension and the random vector composed of the remaining $d - 1$ dimensions. We reported the value averaged over the estimates from the d dimensions.

Results. The MSE and Pearson correlation for the Tiny-ImageNet experiments are reported in Figure 3. The methods trained with linear and non-linear *dependency predictors* both converge to low Pearson correlation coefficients of respectively 0.0107 and 0.0088, and the reconstruction error converges to a value of one for both dependency networks. We further estimate the distance correlation: the approach with non-linear *dependency predictors* reached a lower squared distance correlation than the linear variant, with average values of 5.7×10^{-4} and 2.9×10^{-3} respectively. On the larger ImageNet dataset, the MSE again converges to one and the final squared distance correlation is only 2.1×10^{-4} . These results support the convergence hypothesis.

6.2. Redundancy Minimization on Synthetic Data

This section investigates the impact of our algorithm on redundancy reduction in two different applications: classification and self-supervised learning. To ease the analysis of the representations, both methods were trained on a synthetic dataset for which the latent factors are known.

Clevr-4 dataset. The Clevr-4 (Vaze et al., 2024) dataset is an extension of the CLEVR dataset (Johnson et al., 2017). It comprises 100,000 synthetic images representing 3D objects of various shapes, colors, textures, and counts. Each taxonomy has 10 classes. The label for one taxonomy is sampled uniformly and independently from the others, which means that knowing the label for one taxonomy provides no information about the other taxonomies.

Evaluation protocols. We investigated generalization capabilities by training a classifier on one taxonomy (*shape*) and evaluating its accuracy on the remaining taxonomies to assess if representations encode features beyond the ones relevant to the training classes. The model is compared with a baseline classifier trained without the adversarial objective. We evaluate the accuracy with a simple

weighted-nearest neighbor (kNN) classifier trained on top of frozen features following common practice in SSL (Wu et al., 2018; Caron et al., 2021). The kNN algorithm classifies predictions based on the majority class of their nearest neighbors in the embedding space, providing an easy way to assess the clustering quality for every taxonomy. Similarly, the SSL approach is evaluated with a kNN classifier on the four taxonomies.

Implementation details. Both the supervised and SSL models are trained for 200 epochs. We apply two data augmentations during training: random horizontal flipping and random cropping by keeping at least 60% of the image area, then resizing to 224×224 pixels. We train ResNet-18 encoders and two-layer *dependency predictors*. The networks are trained alternately, with one step for each network per iteration. We set the loss coefficient in both settings to $\lambda = 5$. More details are provided in Appendix G.2. We trained the adversarial networks of the classification and SSL models with respectively an l1 reconstruction loss with a margin of $\alpha = 0.4$ and an MSE reconstruction loss on the standardized representations. The two problem formulations are further discussed and compared in Appendix B.1.

Results on classification. We first compared our regularized classifier to the baseline classifier. Table 1 (top part) reports the validation accuracy and feature correlation. The embedding dimensions of the baseline are highly correlated, with an average squared distance correlation of 0.409. Furthermore, the performance on the taxonomies for which the model received no supervision is low, which was expected since the model was not incentivized to retain information about the remaining taxonomies. When combining the cross-entropy loss with our adversarial objective, the correlation drops to 0.067 and the accuracy on the *texture* and *color* taxonomies rises significantly. These results suggest that the adversarial objective reduces redundancy, leading to representations that generalize better.

Results on SSL. We then compared the SSL approach to two popular frameworks: SimCLR (Chen et al., 2020) and VICReg (Bardes et al., 2021). We re-implemented and extensively tuned the two models. We considered variants with and without projection heads. A detailed description of the hyper-parameters tuning is provided in Appendix H and the best-performing models are reported in Table 1 (bottom part). Without the labels from the *shape* taxonomy, our approach still learns rich representations according to the high accuracy on *shape*, *texture*, and *color*. The linear decorrelation method (VICReg) performs similarly, while the contrastive learning method (SimCLR) performs much worse. These results suggest that decorrelation is an effective approach to SSL and that, in this simple setting, linear decorrelation on high-dimensional representations ($d = 512$) is sufficient for achieving high accuracy.

Table 1: kNN evaluation on the Clevr-4 dataset for two different tasks: classification and self-supervised learning. On classification, our method generalizes beyond the training taxonomy. It also learns strong representations when combined with invariance to data augmentations.

method	kNN top-1 accuracy [%]				mean \mathcal{R}^2
	shape	texture	color	count	
<i>supervised classification (with shape labels)</i>					
cross-entropy (baseline)	100.0	25.0	16.4	36.1	0.409
cross-entropy + ADMin (ours)	100.0	83.7	100.0	39.6	0.067
<i>self-supervised learning (no labels)</i>					
invariance + "push" (SimCLR)	58.8	50.3	91.6	28.4	0.029
invariance + cov. + var. (VICReg)	93.1	89.2	99.5	27.5	0.035
invariance + ADMin (ours)	93.8	88.5	100.0	30.6	0.081

Table 2: Linear evaluation of SSL techniques trained with a ResNet-50 backbone on the ImageNet-1k dataset.

method	acc. [%]
MoCo (He et al., 2020)	60.6
SimCLR (Chen et al., 2020)	69.3
Barlow Twins (Zbontar et al., 2021)	73.2
VICReg (Bardes et al., 2021)	73.2
BYOL (Grill et al., 2020)	74.3
DINO (Caron et al., 2021)	75.3
RELICv2 (Tomasev et al., 2022)	77.1
Ours	63.2

6.3. Validation of the SSL approach on ImageNet

We then investigated if our method still learns useful representations when the training data distribution does not exhibit independence among its underlying latent factors³.

ImageNet dataset. We trained our SSL technique on the Imagenet-1k dataset (Deng et al., 2009), a standard benchmark dataset for SSL. It contains 1,281,167 training images across 1000 classes. This dataset provides a diverse image collection for evaluating our method on real-world data.

Implementation and evaluation. We trained a ResNet-50 backbone with a three-layer projection head with output dimension 512, and two-layer *dependency predictors* on the standardized representations. At evaluation, the projection head is discarded and the representations’ quality is evaluated by training a linear classifier on top of the backbone with frozen weights. The detailed experimental setup is described in Appendix G.3.

Results and discussion. The main SSL techniques are compared in Table 2. After 100 epochs, the average squared distance correlation of our method is 0.015, which

³Take for instance the concepts of road and car. While the concepts are distinct, they are likely to often co-appear in the dataset and are therefore correlated.

demonstrates the algorithm successfully prevented dimensional collapse (Jing et al., 2022). Furthermore, the approach reaches a reasonably high accuracy, suggesting that it can be used even on real-world data (see Appendix E for a qualitative evaluation). However, its performance lags behind state-of-the-art approaches. This gap may be attributed to the fact that most gains in current techniques stem from inductive biases induced by the invariance to carefully designed data augmentations. Our strong nonlinear and mutual dependence minimization term might force the model to compromise when jointly optimizing both objectives (Li et al., 2019). Future work could investigate alternatives to invariance that would better leverage our algorithm’s ability to reduce all dependencies/redundancies.

7. Conclusion

This work introduced an algorithm to minimize the dependence among feature dimensions of a neural network. Its standardized formulation leads to stable training and empirically converges to minimally dependent dimensions. We additionally introduced a margin loss formulation allowing for controlled redundancy levels and validated experimentally that it could benefit certain applications. The algorithm’s applications include: extending PCA to nonlinear decorrelation (PICA), classifier regularization for improved generalization, and learning minimally redundant representations in SSL.

Limitations and future work. Some applications require careful tuning to balance interdependence minimization and task-specific performance, highlighting the need to further study the training dynamics and trade-offs. Other promising areas for future work include exploring how our approach’s generalization capabilities can be leveraged for out-of-distribution detection, as well as independence as a property for representations’ interpretability.

Impact Statement

This paper presents work that aims to advance the field of Machine Learning. There are many potential societal consequences of our work, none of which we feel must be specifically highlighted here.

References

- Back, A. D. and Weigend, A. S. A first application of independent component analysis to extracting structure from stock returns. *International journal of neural systems*, 8 (04):473–484, 1997.
- Baldi, P. and Hornik, K. Neural networks and principal component analysis: Learning from examples without local minima. *Neural networks*, 2(1):53–58, 1989.
- Bardes, A., Ponce, J., and LeCun, Y. Vicreg: Variance-invariance-covariance regularization for self-supervised learning. In *International Conference on Learning Representations*, 2021.
- Belghazi, M. I., Baratin, A., Rajeshwar, S., Ozair, S., Bengio, Y., Courville, A., and Hjelm, D. Mutual information neural estimation. In *International conference on machine learning*, pp. 531–540. PMLR, 2018.
- Bell, A. J. and Sejnowski, T. J. An information-maximization approach to blind separation and blind deconvolution. *Neural computation*, 7(6):1129–1159, 1995.
- Bengio, Y., Courville, A., and Vincent, P. Representation learning: A review and new perspectives. *IEEE transactions on pattern analysis and machine intelligence*, 35 (8):1798–1828, 2013.
- Bordes, F., Balestriero, R., Garrido, Q., Bardes, A., and Vincent, P. Guillotine regularization: Improving deep networks generalization by removing their head. *arXiv preprint arXiv:2206.13378*, 13, 2022.
- Brakel, P. and Bengio, Y. Learning independent features with adversarial nets for non-linear ica. *arXiv preprint arXiv:1710.05050*, 2017.
- Buchholz, S., Besserve, M., and Schölkopf, B. Function classes for identifiable nonlinear independent component analysis. *Advances in Neural Information Processing Systems*, 35:16946–16961, 2022.
- Burgess, C. P., Higgins, I., Pal, A., Matthey, L., Watters, N., Desjardins, G., and Lerchner, A. Understanding disentangling in β -vae. *arXiv preprint arXiv:1804.03599*, 2018.
- Caron, M., Touvron, H., Misra, I., Jégou, H., Mairal, J., Bojanowski, P., and Joulin, A. Emerging properties in self-supervised vision transformers. In *Proceedings of the IEEE/CVF international conference on computer vision*, pp. 9650–9660, 2021.
- Chen, R. T., Li, X., Grosse, R. B., and Duvenaud, D. K. Isolating sources of disentanglement in variational autoencoders. *Advances in neural information processing systems*, 31, 2018.
- Chen, T., Kornblith, S., Norouzi, M., and Hinton, G. A simple framework for contrastive learning of visual representations. In *International conference on machine learning*, pp. 1597–1607. PMLR, 2020.
- Chen, X., Duan, Y., Houthoofd, R., Schulman, J., Sutskever, I., and Abbeel, P. Infogan: Interpretable representation learning by information maximizing generative adversarial nets. *Advances in neural information processing systems*, 29, 2016.
- Cortes, C. Support-vector networks. *Machine Learning*, 1995.
- Cybenko, G. Approximation by superpositions of a sigmoidal function. *Mathematics of control, signals and systems*, 2(4):303–314, 1989.
- Darmois, G. Analyse des liaisons de probabilité. In *Proc. Int. Stat. Conferences 1947*, pp. 231, 1951.
- Deng, J., Dong, W., Socher, R., Li, L.-J., Li, K., and Fei-Fei, L. Imagenet: A large-scale hierarchical image database. In *2009 IEEE conference on computer vision and pattern recognition*, pp. 248–255. IEEE, 2009.
- Driscoll, M. F. On pairwise and mutual independence: characterizations of rectangular distributions. *Journal of the American Statistical Association*, 73(362):432–433, 1978.
- Ermolov, A., Siarohin, A., Sangineto, E., and Sebe, N. Whitening for self-supervised representation learning. In *International conference on machine learning*, pp. 3015–3024. PMLR, 2021.
- Goodfellow, I., Pouget-Abadie, J., Mirza, M., Xu, B., Warde-Farley, D., Ozair, S., Courville, A., and Bengio, Y. Generative adversarial nets. *Advances in neural information processing systems*, 27, 2014.
- Goyal, P. Accurate, large minibatch sgd: training imagenet in 1 hour. *arXiv preprint arXiv:1706.02677*, 2017.
- Grill, J.-B., Strub, F., Altché, F., Tallec, C., Richemond, P., Buchatskaya, E., Doersch, C., Avila Pires, B., Guo, Z., Gheshlaghi Azar, M., et al. Bootstrap your own

- latent-a new approach to self-supervised learning. *Advances in neural information processing systems*, 33: 21271–21284, 2020.
- He, K., Zhang, X., Ren, S., and Sun, J. Deep residual learning for image recognition. In *Proceedings of the IEEE conference on computer vision and pattern recognition*, pp. 770–778, 2016.
- He, K., Fan, H., Wu, Y., Xie, S., and Girshick, R. Momentum contrast for unsupervised visual representation learning. In *Proceedings of the IEEE/CVF conference on computer vision and pattern recognition*, pp. 9729–9738, 2020.
- Hendrycks, D. and Gimpel, K. Gaussian error linear units (gelus). *arXiv preprint arXiv:1606.08415*, 2016.
- Higgins, I., Matthey, L., Pal, A., Burgess, C., Glorot, X., Botvinick, M., Mohamed, S., and Lerchner, A. beta-vaes: Learning basic visual concepts with a constrained variational framework. In *International Conference on Learning Representations*, 2017.
- Hinton, G. E. and Salakhutdinov, R. R. Reducing the dimensionality of data with neural networks. *science*, 313 (5786):504–507, 2006.
- Hinton, G. E., Osindero, S., and Teh, Y.-W. A fast learning algorithm for deep belief nets. *Neural computation*, 18 (7):1527–1554, 2006.
- Hjelm, R. D., Fedorov, A., Lavoie-Marchildon, S., Grewal, K., Bachman, P., Trischler, A., and Bengio, Y. Learning deep representations by mutual information estimation and maximization. In *International Conference on Learning Representations*, 2019.
- Hornik, K., Stinchcombe, M., and White, H. Multilayer feedforward networks are universal approximators. *Neural networks*, 2(5):359–366, 1989.
- Hotelling, H. Analysis of a complex of statistical variables into principal components. *Journal of educational psychology*, 24(6):417, 1933.
- Hua, T., Wang, W., Xue, Z., Ren, S., Wang, Y., and Zhao, H. On feature decorrelation in self-supervised learning. In *Proceedings of the IEEE/CVF International Conference on Computer Vision*, pp. 9598–9608, 2021.
- Huang, L., Yang, D., Lang, B., and Deng, J. Decorrelated batch normalization. In *Proceedings of the IEEE Conference on Computer Vision and Pattern Recognition*, pp. 791–800, 2018.
- Hyvarinen, A. and Morioka, H. Unsupervised feature extraction by time-contrastive learning and nonlinear ica. *Advances in neural information processing systems*, 29, 2016.
- Hyvärinen, A. and Oja, E. Independent component analysis: algorithms and applications. *Neural networks*, 13 (4-5):411–430, 2000.
- Ioffe, S. and Szegedy, C. Batch normalization: Accelerating deep network training by reducing internal covariate shift. In *International conference on machine learning*, pp. 448–456. pmlr, 2015.
- Jing, L., Vincent, P., LeCun, Y., and Tian, Y. Understanding dimensional collapse in contrastive self-supervised learning. In *International Conference on Learning Representations*, 2022.
- Johnson, J., Hariharan, B., Van Der Maaten, L., Fei-Fei, L., Lawrence Zitnick, C., and Girshick, R. Clevr: A diagnostic dataset for compositional language and elementary visual reasoning. In *Proceedings of the IEEE conference on computer vision and pattern recognition*, pp. 2901–2910, 2017.
- Jutten, C. and Herault, J. Blind separation of sources, part i: An adaptive algorithm based on neuromimetic architecture. *Signal processing*, 24(1):1–10, 1991.
- Jutten, C. and Karhunen, J. Advances in blind source separation (bss) and independent component analysis (ica) for nonlinear mixtures. *International journal of neural systems*, 14:267–92, 11 2004.
- Khemakhem, I., Kingma, D., Monti, R., and Hyvarinen, A. Variational autoencoders and nonlinear ica: A unifying framework. In *International conference on artificial intelligence and statistics*, pp. 2207–2217. PMLR, 2020.
- Kim, H. and Mnih, A. Disentangling by factorising. In *International conference on machine learning*, pp. 2649–2658. PMLR, 2018.
- Kingma, D. P. Auto-encoding variational bayes. *arXiv preprint arXiv:1312.6114*, 2013.
- Kramer, M. A. Nonlinear principal component analysis using autoassociative neural networks. *AICHE journal*, 37 (2):233–243, 1991.
- Krizhevsky, A., Sutskever, I., and Hinton, G. E. Imagenet classification with deep convolutional neural networks. *Advances in neural information processing systems*, 25, 2012.
- Le, Y. and Yang, X. Tiny imagenet visual recognition challenge. *CS 231N*, 7(7):3, 2015.

- Leshno, M., Lin, V. Y., Pinkus, A., and Schocken, S. Multilayer feedforward networks with a nonpolynomial activation function can approximate any function. *Neural networks*, 6(6):861–867, 1993.
- Li, Z., Tang, Y., Li, W., and He, Y. Learning disentangled representation with pairwise independence. In *Proceedings of the AAAI conference on artificial intelligence*, volume 33, pp. 4245–4252, 2019.
- Linsker, R. An application of the principle of maximum information preservation to linear systems. *Advances in neural information processing systems*, 1, 1988.
- Locatello, F., Bauer, S., Lucic, M., Raetsch, G., Gelly, S., Schölkopf, B., and Bachem, O. Challenging common assumptions in the unsupervised learning of disentangled representations. In *international conference on machine learning*, pp. 4114–4124. PMLR, 2019.
- Loshchilov, I. and Hutter, F. Sgdr: Stochastic gradient descent with warm restarts. *arXiv preprint arXiv:1608.03983*, 2016.
- Mialon, G., Balestriero, R., and LeCun, Y. Variance covariance regularization enforces pairwise independence in self-supervised representations. *arXiv preprint arXiv:2209.14905*, 2022.
- Pearson, K. Liii. on lines and planes of closest fit to systems of points in space. *The London, Edinburgh, and Dublin philosophical magazine and journal of science*, 2(11): 559–572, 1901.
- Pedregosa, F., Varoquaux, G., Gramfort, A., Michel, V., Thirion, B., Grisel, O., Blondel, M., Prettenhofer, P., Weiss, R., Dubourg, V., Vanderplas, J., Passos, A., Cournapeau, D., Brucher, M., Perrot, M., and Duchesnay, E. Scikit-learn: Machine learning in Python. *Journal of Machine Learning Research*, 12:2825–2830, 2011.
- Ramos-Carreño, C. and Torrecilla, J. L. dcor: Distance correlation and energy statistics in Python. *SoftwareX*, 22, 2 2023. doi: 10.1016/j.softx.2023.101326. URL <https://www.sciencedirect.com/science/article/pii/S2352711023000225>.
- Rumelhart, D. E., Hinton, G. E., and Williams, R. J. Learning internal representations by error propagation, parallel distributed processing, explorations in the microstructure of cognition, ed. de rumelhart and j. mcclelland. vol. 1. 1986. *Biometrika*, 71(599-607):6, 1986a.
- Rumelhart, D. E., Hinton, G. E., and Williams, R. J. Learning representations by back-propagating errors. *nature*, 323(6088):533–536, 1986b.
- Székely, G. J., Rizzo, M. L., and Bakirov, N. K. Measuring and testing dependence by correlation of distances. *The Annals of Statistics*, 35(6):2769, 2007.
- Taleb, A. and Jutten, C. Source separation in post-nonlinear mixtures. *IEEE Transactions on signal processing*, 47(10):2807–2820, 1999.
- Tomasev, N., Bica, I., McWilliams, B., Buesing, L. H., Pascanu, R., Blundell, C., and Mitrovic, J. Pushing the limits of self-supervised resnets: Can we outperform supervised learning without labels on imagenet? In *First Workshop on Pre-training: Perspectives, Pitfalls, and Paths Forward at ICML 2022*, 2022.
- Tsochantaridis, I., Joachims, T., Hofmann, T., Altun, Y., and Singer, Y. Large margin methods for structured and interdependent output variables. *Journal of machine learning research*, 6(9), 2005.
- Vaze, S., Vedaldi, A., and Zisserman, A. No representation rules them all in category discovery. *Advances in Neural Information Processing Systems*, 36, 2024.
- Wu, Z., Xiong, Y., Yu, S. X., and Lin, D. Unsupervised feature learning via non-parametric instance discrimination. In *Proceedings of the IEEE conference on computer vision and pattern recognition*, pp. 3733–3742, 2018.
- Yao, F., Coquery, J., and Lê Cao, K.-A. Independent principal component analysis for biologically meaningful dimension reduction of large biological data sets. *BMC bioinformatics*, 13:1–15, 2012.
- You, Y., Gitman, I., and Ginsburg, B. Large batch training of convolutional networks. *arXiv preprint arXiv:1708.03888*, 2017.
- Zbontar, J., Jing, L., Misra, I., LeCun, Y., and Deny, S. Barlow twins: Self-supervised learning via redundancy reduction. In *International conference on machine learning*, pp. 12310–12320. PMLR, 2021.

A. Principal and Independent Component Analysis (PICA)

A.1. Empirical Study of Example 3

In Example 3, the solution that maximizes the explained variance under the zero correlation constraint is $\mathbf{z}_{\text{PCA}} = [x_1, x_2]^T$, with a total variance of $\mathbb{V}[\mathbf{z}_{\text{PCA}}] = 25 + 4.5 = 29.5$. However, this is not a solution to PICA since $x_1 = 5v_1$ and $x_2 = 3 \cos 2\pi v_1 / \sqrt{3}$ are both functions of the same latent factor v_1 . The solution to PICA is thus $\mathbf{z}_{\text{PICA}} = [x_1, x_3]^T$, with a total explained variance of $\mathbb{V}[\mathbf{z}_{\text{PICA}}] = 25 + 1 = 26$. Attention should be drawn to the fact that the explained variance of PICA is always smaller or equal to the PCA decomposition. The equality occurs only when the highest variance uncorrelated combination of the inputs is mutually (and non-linearly) independent.

We empirically study this example by comparing the solutions to four different implementations:

1. the PCA decomposition solved with a Singular Value Decomposition. For this example, we rely on the *scikit-learn* (Pedregosa et al., 2011) implementation: <https://scikit-learn.org/1.6/modules/generated/sklearn.decomposition.PCA.html>.
2. the PCA decomposition implemented with a linear autoencoder and a covariance minimization objective. This approach is similar to (Mialon et al., 2022) but without their variance regularization term.
3. the PCA decomposition implemented with a linear autoencoder and our standardized adversarial objective with linear dependency predictors.
4. the PICA decomposition implemented with a linear autoencoder and our standardized adversarial objective with nonlinear dependency predictors.

Implementation details. We train methods (2) to (4) for 5000 steps. We generate 512 observations \mathbf{x} by sampling from the uniform latent factors \mathbf{v} at every iteration. The encoder is implemented with a projection $\mathbf{W}^T \in \mathbb{R}^{3 \times 2}$ and the decoder uses the same matrix \mathbf{W} . The autoencoders and dependency predictors are trained with the Adam optimizer, with learning rates of respectively $5 \cdot 10^{-3}$ and $2 \cdot 10^{-2}$. The training steps ratios are set to $k = 16$. The covariance/dependence minimization loss coefficients are set to $\lambda = 1$, while the reconstruction loss coefficient is set to 0.02. This weighting strategy aims to push the method not to compromise the covariance/dependence for a decreased reconstruction error.

The PCA implementations from (1), (2) and (3) find respectively:

$$W_{\text{PCA},1} \approx \begin{bmatrix} 1 & 0 & 0 \\ 0 & 1 & 0 \end{bmatrix} \quad W_{\text{PCA},2} \approx \begin{bmatrix} 0.00 & 1.00 & -0.01 \\ 1.00 & -0.01 & 0.00 \end{bmatrix} \quad W_{\text{PCA},3} \approx \begin{bmatrix} 0.00 & 1.00 & 0.01 \\ -1.00 & 0.00 & 0.01 \end{bmatrix} \quad (10)$$

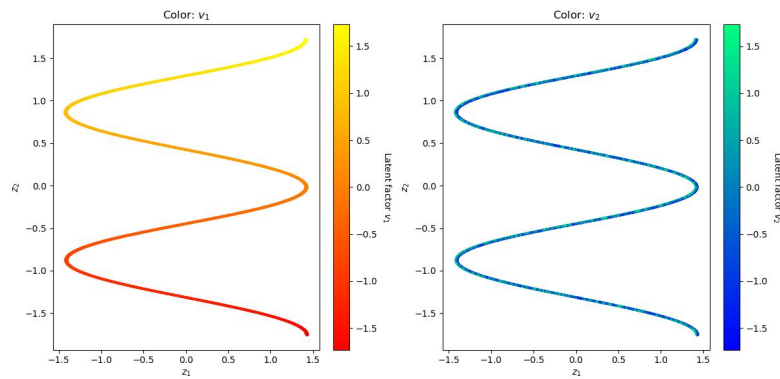
In line with theory, the three PCA implementations thus extracted the first two observed variables x_1 and x_2 . For implementations (1) to (3), the total explained variances for the representations \mathbf{z} are all approximately equal to 29.5 and covariance matrices are close to diagonal. However, the learned latent dimensions are not independent, with a distance correlation of $\mathcal{R}(z_1, z_2) \approx 0.25$. The methods accurately reconstruct the first two observed variables x_1 and x_2 , and achieve an average reconstruction error of 1 for x_3 . It should be emphasized that this average error corresponds to the variance of x_3 .

The representations \mathbf{z} for experiments (2) and (3) are shown in Figure 4a and Figure 4b. The abscissa and ordinate depict the learned latent variables z_1 and z_2 , while the color of the predictions indicates the true value of the true latent factors v_1 (left figure) and v_2 (right figure). The distributions align with our previous finding and illustrate that none of the PCA implementations encoded the latent factor v_2 .

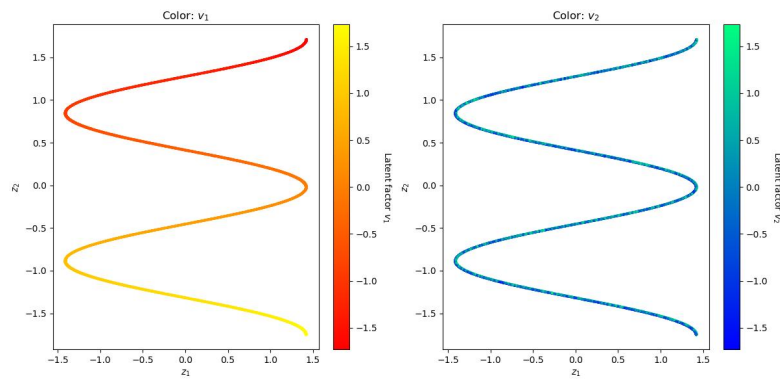
On the contrary, the PICA implementation (4) learns:

$$W_{\text{PICA}} \approx \begin{bmatrix} 1.00 & 0.00 & 0.01 \\ 0.00 & -0.01 & 1.00 \end{bmatrix} \quad (11)$$

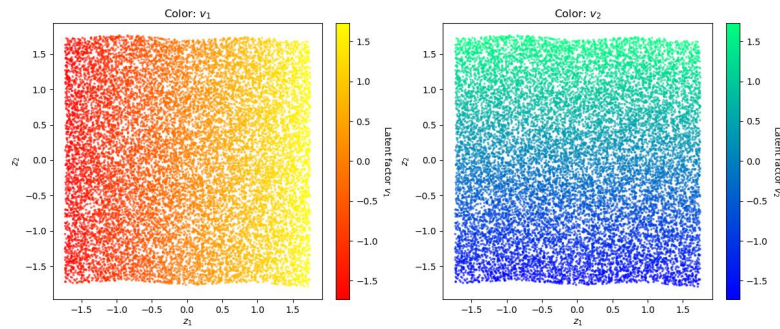
The average reconstruction error is 4.46, which approximately equals the second dimension’s variance. Furthermore, the distance correlation between the two learned representations is $\mathcal{R}(z_1, z_2) \approx 0.008$. These empirical results validate that the PICA reduction captured the two independent latent factors v_1 and v_2 . Furthermore, the method could not reconstruct x_2 since it is implemented with a linear autoencoder. The distribution of the learned representations \mathbf{z} is shown in Figure 4c.



(a) PCA reduction implemented with a linear autoencoder and a covariance regularization term.



(b) PCA reduction implemented with a linear autoencoder and linear *dependency predictors*.



(c) PICA reduction implemented with a linear autoencoder and nonlinear *dependency predictors*.

Figure 4: Learned representations \mathbf{z} . The colors indicate the value of the original latent factors v_1 (left) and v_2 (right).

A.2. Nonlinear Principal and Independent Component Analysis

The Non-Linear Principal Component Analysis (NLPCA) extended PCA to non-linear transformations. It was introduced by (Kramer, 1991) as an auto-encoder learning the identity mapping. The architecture included an intermediate "bottleneck" representation, forcing the network to learn low-dimensional data representations. The original architecture was a four-layer feed-forward neural network with sigmoid activation functions. Following this definition, one can learn a NLPCA reduction by training an encoder $f_\theta : \mathbb{R}^l \rightarrow \mathbb{R}^d$ and a decoder $g_\psi : \mathbb{R}^d \rightarrow \mathbb{R}^l$ to minimize the reconstruction error:

$$\min_{\theta, \psi} \frac{1}{N} \sum_{i=1}^N \|\mathbf{x}^{(i)} - g_\psi(f_\theta(\mathbf{x}^{(i)}))\|_2^2 \quad (12)$$

One may assume that a solution with minimal reconstruction error should exhibit low redundancy in the bottleneck representation. Yet, equation 12 does not explicitly push the bottleneck representation to have uncorrelated dimensions. Therefore, starting from the encoder-decoder architecture from the equation 12, we add the ADMin objective by following the development from Section 5.1:

$$\min_{\theta, \psi} \frac{1}{N} \sum_{i=1}^N \|\mathbf{x}^{(i)} - g_\psi(f_\theta(\mathbf{x}^{(i)}))\|_2^2 + \lambda \mathcal{L}_{\text{adv}}(\mathbf{z}^{(i)}, \hat{\mathbf{z}}^{(i)}) \quad (13)$$

where $\mathbf{z}^{(i)} = f_\theta(\mathbf{x}^{(i)})$ is the bottleneck representation and $\hat{\mathbf{z}}_j^{(i)} = h_{\phi_j}(z_1^{(i)}, \dots, z_{j-1}^{(i)}, z_{j+1}^{(i)}, \dots, z_d^{(i)})$ is the prediction from the j -th *dependency predictor*. We denote this extension as *Non-Linear Principal and Independent Component Analysis* (NLPICA) since it is an extension of the NLPCA reduction with an additional objective pushing the representations to have minimally interdependent dimensions.

Note that the solution to the NLPICA reduction is not unique. In fact, research in nonlinear independent component analysis (NLICA) demonstrated that there are countless ways to transform independent variables while maintaining statistical independence (Darmois, 1951; Jutten & Karhunen, 2004). These transformations can involve complex mixing functions that result in representations that may be challenging to interpret or exhibit undesirable properties for certain applications. For examples of mixing transformations, we refer to (Taleb & Jutten, 1999). Despite this limitation, the problem can be made identifiable again with additional assumptions such as temporal non-stationarity (Hyvarinen & Morioka, 2016), a conditionally factorized prior distribution over the latent variables of a VAE (Khemakhem et al., 2020) or constraining the function class with constraints on their partial derivatives (Buchholz et al., 2022).

B. Ablation Studies

B.1. Reduncancy and Downstream Performance

This section assesses the impact of the two problem formulations on downstream performance and correlation. We train the classification method from Section 6.2 in three different settings: with standardization of the representations, without standardization but with a margin, and with neither of these. From the results reported in Table 3, it can be observed that the standardized version (first row) achieves by far the lowest correlation level, but its accuracy on the *texture*, *color* and *count* taxonomies is not better than the baseline from Table 1. In contrast, the margin loss (second row) performs well on all taxonomies. Finally, the method with neither a margin nor standardization (third row) performs poorly on the unknown taxonomies and has a much higher correlation level. This can be explained by analyzing that this method indefinitely increased the representation norm instead of decorrelating the variables, reaching an average representation norm of 584.4, while the version with a margin stabilized to around 56.1. We finally report the average accuracy and correlation for different margin values in Figure 5. The figure demonstrates that accuracy increases with the margin up to a margin of 0.4, but that too large margins lead to poor performance on the unknown taxonomies.

C. Independence and Correlation

C.1. Distance Correlation

Distance correlation (Székely et al., 2007) is a non-negative coefficient that characterizes both linear and nonlinear correlations between random vectors. Let x_1 and x_2 be two random vectors with finite first moments, their respective characteristic

Table 3: Impact of different adversarial loss formulations on a classification problem. The classifiers are trained on the *shape* taxonomy from the Clevr-4 dataset.

formulation	kNN top-1 accuracy						mean \mathcal{R}^2
	std.	margin	shape	texture	color	count	
✓	✗		100.0	21.2	16.9	22.1	0.009
✗		0.4	100.0	83.7	100.0	39.6	0.068
✗	✗		100.0	18.4	40.4	32.2	0.287

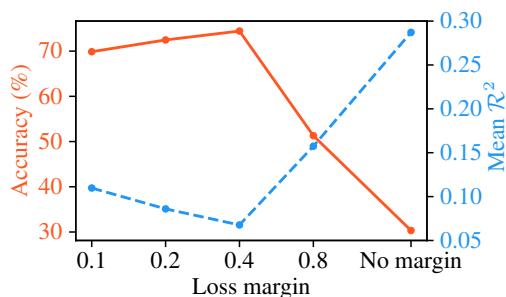


Figure 5: Influence of the loss margin on the correlation and accuracy for classification models trained on the Clevr-4 dataset. The models are trained on the *shape* taxonomy and the kNN accuracy is averaged over the three remaining taxonomies.

functions be denoted ψ_{x_1} and ψ_{x_2} , and their joint characteristic function be denoted ψ_{x_1, x_2} . Distance covariance measures the distance between their joint characteristic function and the product of the marginal characteristic functions:

$$\mathcal{V}^2(x_1, x_2) = \int_{\mathbb{R}^{p+q}} |\psi_{x_1, x_2}(t, s) - \psi_{x_1}(t)\psi_{x_2}(s)|^2 w(t, s) dt ds \tag{14}$$

where $w(t, s)$ is a positive weight function and characteristic functions are $\psi_x(t) = \mathbb{E}[e^{itx}]$. Analogous to Pearson correlation, the squared distance correlation \mathcal{R}^2 is defined by: $\mathcal{R}^2(x_1, x_2) = \mathcal{V}^2(x_1, x_2) / \sqrt{\mathcal{V}^2(x_1, x_1)\mathcal{V}^2(x_2, x_2)}$ if $\mathcal{V}^2(x_1, x_1)\mathcal{V}^2(x_2, x_2) > 0$ and 0 otherwise.

We refer to the original paper (Székely et al., 2007) for the empirical estimation of distance correlation and to the library (Ramos-Carreño & Torrecilla, 2023) for its implementation.

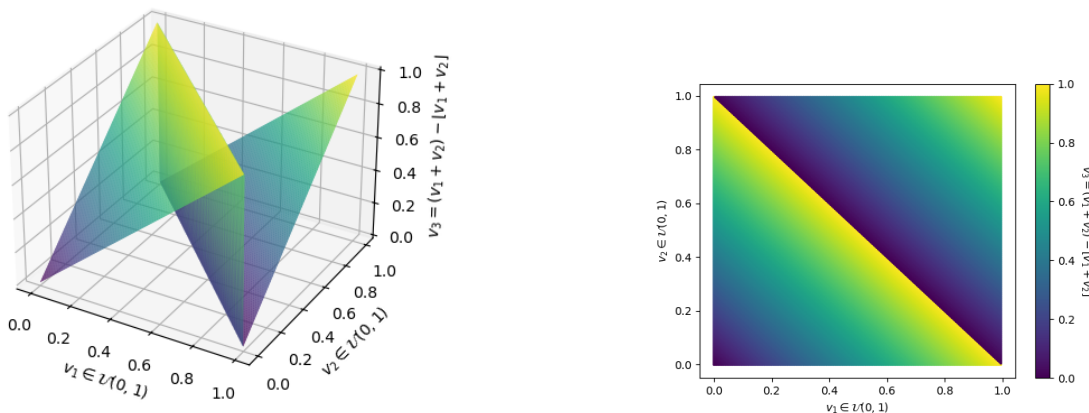


Figure 6: Illustration of Example 4: the random variables x_1 , x_2 and x_3 are all mutually dependent despite being all pairwise independent.

C.2. Pairwise and Mutual Independence

Example 4. Let two random variables x_1 and x_2 be drawn from uniform distributions in the interval $[0, 1]$. Then, define the random variable $x_3 = x_1 + x_2 - \lfloor x_1 + x_2 \rfloor$ where $\lfloor \cdot \rfloor$ denotes the integral part of the value (e.g., $\lfloor 3.14 \rfloor = 3$). The random variable x_3 is uniformly distributed on $[0, 1]$ (see Figure 6) and the pairs $\{x_1, x_2\}$, $\{x_1, x_3\}$ and $\{x_2, x_3\}$ are pairwise independent. Still, the variables are not mutually independent since the uncertainty of x_3 is zero when the random vector $x_{-3} = [x_1, x_2]^T$ is known.

D. Algorithm

Algorithm 1 Training algorithm for the adversarial dependence minimization

```

1: for number of training iterations do
2:   for k steps do
3:     Sample a minibatch of n examples  $\{\mathbf{x}^{(1)}, \mathbf{x}^{(2)}, \dots, \mathbf{x}^{(n)}\}$  from the dataset
4:     Compute the representations from the encoder  $\mathbf{z}^{(i)} = f_{\theta}(\mathbf{x}^{(i)})$  for every sample i
5:     Compute  $\mu_j = \frac{1}{n} \sum_{i=1}^n z_j^{(i)}$  and  $\sigma_j = \frac{1}{n-1} \sum_{i=1}^n (z_j^{(i)} - \mu_j)^2$  for every dimension j
6:     Standardize the representations  $z_j^{(i)} \leftarrow \frac{z_j^{(i)} - \mu_j}{\sigma_j}$ 
7:     Reconstruct the embedding dimensions  $\hat{z}_j^{(i)} = h_{\phi_j}(z_1^{(i)}, \dots, z_{j-1}^{(i)}, z_{j+1}^{(i)}, \dots, z_d^{(i)})$  for every dimension j and every sample i
8:     Update the dependency predictors by gradient descent  $\nabla_{\phi} \frac{1}{n} \sum_{i=1}^n \|\mathbf{z}^{(i)} - \hat{\mathbf{z}}^{(i)}\|_2^2$ 
9:   end for
10:  Sample a minibatch of n examples  $\{\mathbf{x}^{(1)}, \mathbf{x}^{(2)}, \dots, \mathbf{x}^{(n)}\}$  from the dataset
11:  Compute the representations from the encoder  $\mathbf{z}^{(i)} = f_{\theta}(\mathbf{x}^{(i)})$  for every sample i
12:  Compute  $\mu_j = \frac{1}{n} \sum_{i=1}^n z_j^{(i)}$  and  $\sigma_j = \frac{1}{n-1} \sum_{i=1}^n (z_j^{(i)} - \mu_j)^2$  for every dimension j
13:  Standardize the representations  $z_j^{(i)} \leftarrow \frac{z_j^{(i)} - \mu_j}{\sigma_j}$ 
14:  Reconstruct the embedding dimensions  $\hat{z}_j^{(i)} = h_{\phi_j}(z_1^{(i)}, \dots, z_{j-1}^{(i)}, z_{j+1}^{(i)}, \dots, z_d^{(i)})$  for every dimension j and every sample i
15:  Update the encoder by gradient descent  $\nabla_{\theta} 1 - \frac{1}{n} \sum_{i=1}^n \|\mathbf{z}^{(i)} - \hat{\mathbf{z}}^{(i)}\|_2^2$ 
16: end for

```

E. Nearest Neighbors Visualization

We visualize the nearest neighbors for the self-supervised models described in Section 6.2. Figure 7 shows the predicted nearest neighbors for five randomly sampled validation images from the Clevr-4 and ImageNet datasets. The left-most image is the query image, and its nearest neighbors are the training samples whose representations have the highest cosine similarity to the query’s representation. The figure demonstrates that the nearest neighbors visually resemble the query images on both datasets.

F. Architectures

The network architectures for the applications from Section 5 are depicted in Figure 8.

G. Detailed Experimental Setups

We provide here a detailed description of the training settings and hyper-parameters to facilitate the reproducibility of our experimental results.

The encoder and dependence networks are trained alternately, following the algorithm presented in Appendix D. Epochs are counted relative to the encoder, which means that the dependence networks loop through the dataset k times per encoder epoch.

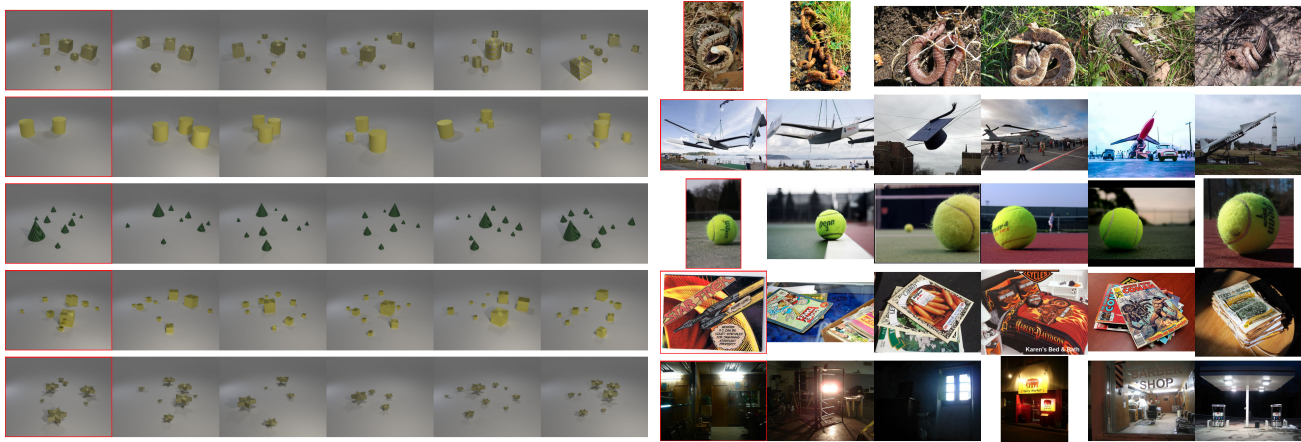


Figure 7: Nearest neighbors visualization for SSL models trained on the Clevr-4 dataset (left) and ImageNet dataset (right). The nearest neighbors visually resemble the query images (highlighted in red).

Dependence networks. Dependence networks are always trained with the same optimizer and schedulers as their respective encoder. The default dependence network is a two-layer fully-connected network with a hidden dimension of size 32 and intermediate GELU (Hendrycks & Gimpel, 2016) activation function. There is no activation function at the output of the network.

G.1. Experimental Setup: Convergence Analysis

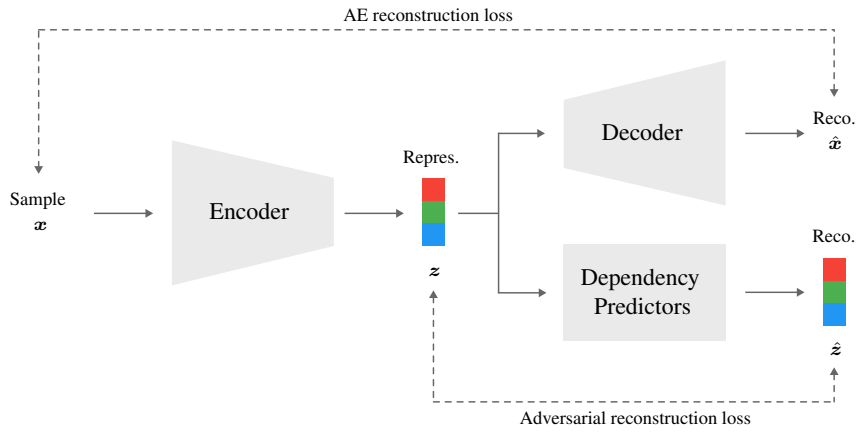
TinyImageNet experiments. We trained two different dependence networks: a linear and a two-layer fully-connected network. Both are trained on standardized representations. The encoder is a ResNet-18 backbone with no projection head. We used the SGD optimizer with a momentum of 0.9, a learning rate of 0.8, a batch size of 256, and no weight decay. No learning rate schedule is used in this setting. The dependence networks are trained with a ratio of $k = 2$ steps with learning rates of respectively 0.04 and 3.2. The models are trained on the TinyImageNet dataset for 100 epochs without data augmentations, but images are normalized with ImageNet mean and standard deviation per-channel values.

ImageNet experiment. We trained two-layer dependence networks on standardized representations. The encoder is a ResNet-18 backbone with a three-layer fully-connected projection head with a hidden dimension of 4096, an output dimension of 512, ReLU activation functions, and intermediate BatchNorm layers. We used the SGD optimizer with a momentum of 0.9, a learning rate of 3.2, a batch size of 1024, and no weight decay. The learning rate follows a cosine decay schedule (Loshchilov & Hutter, 2016) with 10 epochs of linear warmup. The dependence networks are trained with a ratio of $k = 4$ steps with a learning rate of 16. The model is trained on the ImageNet dataset for 50 epochs and follows the same data augmentations as the first views in (Grill et al., 2020).

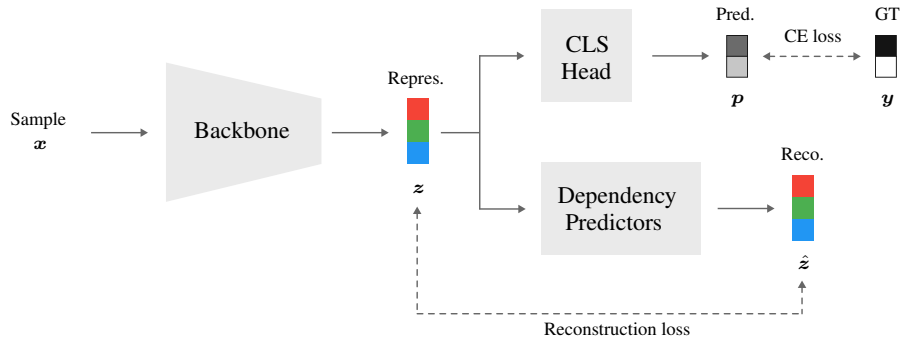
G.2. Experimental Setup: Clevr-4

Classification. The baseline and adversarial approaches are trained with the same set of hyper-parameters, we therefore describe only the adversarial setting. We trained two-layer dependence networks. The encoder is a ResNet-18 backbone with no projection head. We used the SGD optimizer with a momentum of 0.9, a learning rate of 0.1, a batch size of 256, and a weight decay of $2 \cdot 10^{-5}$. The learning rate follows a cosine decay schedule (Loshchilov & Hutter, 2016) with 10 epochs of linear warmup. The dependence networks are trained with a ratio of $k = 1$ steps with a learning rate of 0.3. The adversarial objective is a 11 margin loss on unstandardized representations with margin $\alpha = 0.4$. The task weight is $\lambda = 5$. The models are trained for 200 epochs and data augmentations are described in Section 6.2.

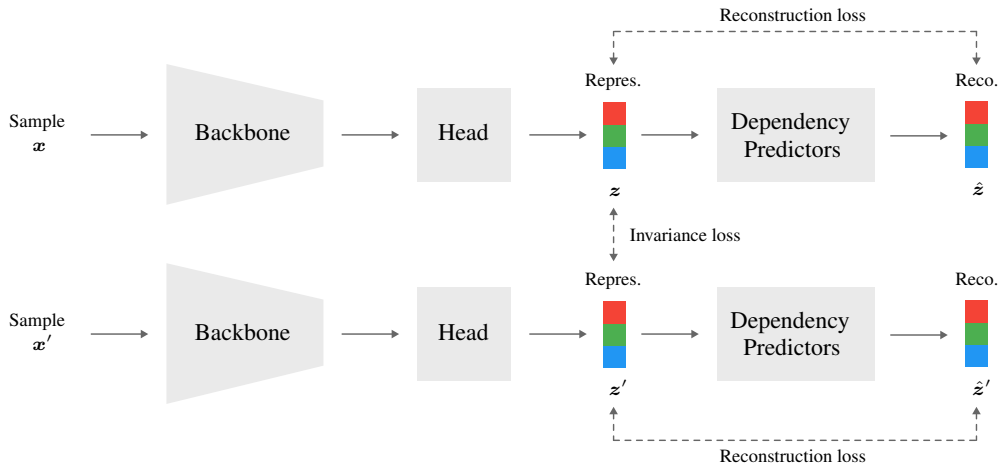
SSL. We trained two-layer dependence networks on standardized representations. The encoder is a ResNet-18 backbone with no projection head. We used the SGD optimizer with a momentum of 0.9, a learning rate of 0.8, a batch size of 256, and a weight decay of $2 \cdot 10^{-5}$. The learning rate follows a cosine decay schedule (Loshchilov & Hutter, 2016) with 10 epochs of linear warmup. The dependence networks are trained with a ratio of $k = 1$ steps with a learning rate of 0.3. The adversarial objective is a 11 margin loss with margin $\alpha = 0.4$. The task weight is $\lambda = 5$. The models are trained for 200



(a) PICA architecture.



(b) Classification architecture.



(c) Self-supervised representation learning architecture.

Figure 8: Illustration of the different applications.

epochs and data augmentations are described in Section 6.2.

G.3. Experimental Setup: ImageNet SSL

We trained two-layer dependence networks on standardized representations. The encoder is a ResNet-50 backbone with a three-layer fully-connected projection head with a hidden dimension of 4096, an output dimension of 512, ReLU activation functions, and intermediate BatchNorm layers. We used the LARS optimizer (You et al., 2017) with a momentum of 0.9, a base learning rate of 1.5 with linear scaling rule (Goyal, 2017), a batch size of 1024, and a weight decay of 10^{-4} . The learning rate follows a cosine decay schedule (Loshchilov & Hutter, 2016) with 10 epochs of linear warmup. The dependence networks are trained with a ratio of $k = 4$ steps with a base learning rate of 6. The model is trained on the ImageNet dataset for 100 epochs and follows the same data augmentations as in (Grill et al., 2020).

Linear evaluation. We followed standard procedure and trained a linear classifier on top of the frozen representations from the backbone. We used the SGD optimizer with a learning rate of 1.5, a weight decay of 10^{-6} , a batch size of 256, and trained for 100 epochs. The learning rate follows a cosine decay schedule (Loshchilov & Hutter, 2016). We applied two data augmentations during training: random horizontal flipping with $p = 0.5$ and random cropping by keeping at least 8% of the image area, followed by resizing to 224×224 pixels. During the evaluation, the images were resized so that the smaller side was 256 pixels wide and then center cropped to 224×224 pixels.

G.4. Experimental Setup: Redundancy Study

The experimental setup is the same as for the classification model from Section 6.2 already described in Appendix G.2. The only difference is that the model trained with standardized representations for reconstruction is trained with a mean squared reconstruction loss. Its dependence networks are trained with a ratio of $k = 2$ steps instead of $k = 1$ since this model did not converge with $k = 1$.

H. Clevr-4 Baselines

This section details the hyper-parameter tuning of the SimCLR and VICReg baselines.

We implemented the models following the original papers from SimCLR (Chen et al., 2020) and VICReg (Bardes et al., 2021). We trained ResNet-18 backbones and trained each model with and without a projection head to find which setup works best for each technique when applied to the Clevr-4 dataset. For a fair comparison, we followed the same experimental setup as for our SSL method: we used the SGD optimizer with a momentum of 0.9, and a weight decay of $2 \cdot 10^{-5}$. The learning rate follows a cosine decay schedule (Loshchilov & Hutter, 2016) with 10 epochs of linear warmup and is scaled with a linear scaling rule (Goyal, 2017).

We ran a grid search on the projection head choice, the learning rate, and the batch size. The models were trained for 80 epochs and the best-performing model was then re-trained for 200 epochs. Its results are reported in Table ?? from Section 6.2.

Results for the grid search on the hyper-parameters from SimCLR and VICReg are reported respectively in Table 4 and in Table 5. We observe that the best-performing model for SimCLR has a projection head, while the VICReg technique works better with no projection head. This observation for VICReg is consistent with findings from our method applied to Clevr-4. This may be because the taxonomies are statistically independent and the augmentations are minimal, reducing the need for a projection head to prevent true invariance to data augmentations (Bordes et al., 2022).

Table 4: Results for the grid-search on SimCLR’s hyper-parameters on the Clevr-4 dataset. *LR* stands for base learning rate and *BS* stands for batch size. The best-performing model is **highlighted**.

head	hyper-parameters			kNN top-1 accuracy			
	output dim.	<i>LR</i>	<i>BS</i>	shape	texture	color	count
Identity	(512)	0.025	256	42.6	40.7	83.1	24.3
Identity	(512)	0.025	512	40.6	40.4	83.1	24.2
Identity	(512)	0.05	256	40.7	39.1	83.9	24.1
Identity	(512)	0.05	512	47.7	39.8	80.8	24.3
Identity	(512)	0.1	256	47.9	40.0	80.4	24.2
Identity	(512)	0.1	512	10.1	9.9	9.8	9.4
Identity	(512)	0.2	256	39.7	34.8	76.8	24.0
Identity	(512)	0.2	512	40.3	32.2	75.4	23.5
Identity	(512)	0.4	256	40.9	31.6	72.0	23.6
Identity	(512)	0.4	512	42.6	29.9	73.3	22.6
Identity	(512)	0.6	256	36.2	28.0	70.2	23.6
Identity	(512)	0.6	512	40.6	31.9	73.4	22.8
MLP	128	0.025	256	57.1	53.5	92.7	29.9
MLP	128	0.025	512	55.6	51.0	90.9	28.2
MLP	128	0.05	256	57.7	51.7	92.0	28.9
MLP	128	0.05	512	55.4	47.3	87.8	27.6
MLP	128	0.1	256	57.6	48.4	89.1	28.0
MLP	128	0.1	512	47.7	41.2	86.4	27.3
MLP	128	0.2	256	48.2	39.2	82.8	27.2
MLP	128	0.2	512	45.9	39.3	84.2	26.5
MLP	128	0.4	256	44.7	34.9	74.7	26.3
MLP	128	0.4	512	46.0	35.6	75.1	26.7
MLP	128	0.6	256	44.0	34.4	73.8	26.6
MLP	128	0.6	512	40.8	37.3	70.4	26.4
MLP	512	0.025	256	47.3	47.7	89.1	29.4
MLP	512	0.025	512	46.7	46.2	89.4	28.4
MLP	512	0.05	256	46.6	45.7	88.0	28.3
MLP	512	0.05	512	46.2	43.7	87.1	28.2
MLP	512	0.1	256	47.0	42.6	84.9	28.2
MLP	512	0.1	512	54.4	44.2	85.7	27.3
MLP	512	0.2	256	44.8	37.9	81.1	27.1
MLP	512	0.2	512	49.4	42.6	79.6	26.3
MLP	512	0.4	256	44.9	38.7	75.7	26.4
MLP	512	0.4	512	46.6	37.0	75.9	26.3
MLP	512	0.6	256	44.4	35.0	75.1	27.4
MLP	512	0.6	512	45.2	34.1	73.3	27.0

Table 5: Results for the grid-search on VICReg’s hyper-parameters on the Clevr-4 dataset. *LR* stands for base learning rate and *BS* stands for batch size. The best-performing model is **highlighted**.

head	hyper-parameters			kNN top-1 accuracy			
	output dim.	<i>LR</i>	<i>BS</i>	shape	texture	color	count
Identity	(512)	0.005	256	82.1	86.7	100.0	28.2
Identity	(512)	0.005	512	88.3	87.4	100.0	26.5
Identity	(512)	0.01	256	86.9	85.3	100.0	34.1
Identity	(512)	0.01	512	91.4	88.6	100.0	27.2
Identity	(512)	0.025	256	84.1	79.4	99.5	29.8
Identity	(512)	0.025	512	86.2	84.3	99.4	31.9
Identity	(512)	0.05	256	73.9	71.0	98.9	26.3
Identity	(512)	0.05	512	81.0	77.5	98.9	28.8
Identity	(512)	0.1	256	72.5	66.9	98.8	24.2
Identity	(512)	0.1	512	60.6	65.0	98.4	23.7
Identity	(512)	0.2	256	63.1	57.0	98.2	22.9
Identity	(512)	0.2	512	51.1	54.8	97.0	20.0
Identity	(512)	0.4	256	44.4	48.3	97.0	22.9
Identity	(512)	0.4	512	50.3	51.2	97.4	23.5
MLP	128	0.005	256	51.0	57.6	99.5	30.4
MLP	128	0.005	512	51.4	61.3	99.0	29.7
MLP	128	0.01	256	44.4	54.9	98.2	29.0
MLP	128	0.01	512	47.7	57.5	98.3	27.7
MLP	128	0.025	256	34.8	51.1	97.0	24.2
MLP	128	0.025	512	42.8	50.6	97.0	25.8
MLP	128	0.05	256	36.1	44.6	95.8	25.0
MLP	128	0.05	512	36.8	49.9	97.3	24.7
MLP	128	0.1	256	31.1	42.3	95.3	24.5
MLP	128	0.1	512	34.3	44.3	96.2	25.2
MLP	128	0.2	256	30.3	40.9	95.8	23.3
MLP	128	0.2	512	31.7	42.7	96.3	23.5
MLP	128	0.4	256	28.1	25.8	94.5	23.2
MLP	128	0.4	512	26.8	14.1	33.3	21.5
MLP	512	0.005	256	63.7	68.3	99.5	30.5
MLP	512	0.005	512	63.8	66.1	99.4	28.4
MLP	512	0.01	256	59.6	63.5	98.7	28.3
MLP	512	0.01	512	61.5	64.3	98.6	26.2
MLP	512	0.025	256	61.2	60.2	97.9	26.6
MLP	512	0.025	512	62.2	62.8	98.0	24.7
MLP	512	0.05	256	59.8	58.5	97.4	25.7
MLP	512	0.05	512	58.6	59.1	97.2	23.9
MLP	512	0.1	256	57.2	57.2	97.1	24.7
MLP	512	0.1	512	57.2	56.8	97.0	23.5
MLP	512	0.2	256	56.9	52.9	96.6	24.5
MLP	512	0.2	512	55.7	54.2	96.8	23.5
MLP	512	0.4	256	46.2	49.0	96.3	23.7
MLP	512	0.4	512	44.1	51.2	96.5	23.0